Rapid Communications | Editors' Suggestion

Emergent spin-1 Haldane gap and ferroelectricity in a frustrated spin-$\frac{1}{2}$ ladder

H. Ueda,[1,2] S. Onoda,[3,4] Y. Yamaguchi,[5] T. Kimura,[6] D. Yoshizawa,[7] T. Morioka,[7] M. Hagiwara,[7] M. Hagihala,[8] M. Soda,[8] T. Masuda,[8] T. Sakakibara,[8] K. Tomiyasu,[9] S. Ohira-Kawamura,[10] K. Nakajima,[10] R. Kajimoto,[10] M. Nakamura,[10] Y. Inamura,[10] N. Reynolds,[11] M. Frontzek,[11,12] J. S. White,[11] M. Hase,[13] and Y. Yasui[14]

[1]*Computational Materials Science Research Team, RIKEN Center for Computational Science (R-CCS), Kobe 650-0047, Japan*
[2]*JST, PRESTO, Kawaguchi, Saitama 332-0012, Japan*
[3]*Condensed Matter Theory Laboratory, RIKEN, Wako, Saitama 351-0198, Japan*
[4]*Quantum Matter Theory Research Team, RIKEN Center for Emergent Matter Science (CEMS), Wako 351-0198, Japan*
[5]*Division of Materials Physics, Graduate School of Engineering Science, Osaka University, Toyonaka, Osaka 560-8531, Japan*
[6]*Department of Advanced Materials Science, Graduate School of Frontier Sciences, The University of Tokyo, Kashiwa 277-8561, Japan*
[7]*Center for Advanced High Magnetic Field Science, Graduate School of Science, Osaka University, Toyonaka, Osaka 560-0043, Japan*
[8]*Institute for Solid State Physics, The University of Tokyo, Kashiwa 277-8581, Japan*
[9]*Department of Physics, Tohoku University, Sendai 980-8578, Japan*
[10]*Materials and Life Science Division, J-PARC Center, Japan Atomic Energy Agency, Tokai 319-1195, Japan*
[11]*Laboratory for Neutron Scattering, Paul Scherrer Institut, CH-5232 Villigen, Switzerland*
[12]*Neutron Scattering Division, Oak Ridge National Laboratory, Oak Ridge, Tennessee 37831, USA*
[13]*National Institute for Materials Science (NIMS), Tsukuba, Ibaraki 305-0047, Japan*
[14]*Department of Physics, School of Science and Technology, Meiji University, Higashi-mita, Tama-ku, Kawasaki 214-8571, Japan*

(Received 19 March 2018; revised manuscript received 20 August 2018; accepted 31 March 2020; published 22 April 2020)

We report experimental and theoretical evidence that $Rb_2Cu_2Mo_3O_{12}$ has a nonmagnetic tetramer ground state of a two-leg ladder comprising antiferromagnetically coupled frustrated spin-$\frac{1}{2}$ chains and exhibits a Haldane spin gap of emergent spin-1 pairs. Three spin excitations split from the spin-1 triplet by a Dzyaloshinskii-Moriya interaction are identified in inelastic neutron-scattering and electron spin resonance spectra. A tiny magnetic field generates ferroelectricity without closing the spin gap, indicating a unique class of ferroelectricity induced by a vector spin chirality order.

DOI: 10.1103/PhysRevB.101.140408

Quantum spin fluctuations offer a source of various nontrivial states including resonating valence bonds and quantum spin liquids [1]. In a one-dimensional (1D) antiferromagnet having only the first-neighbor exchange coupling J_1 [Fig. 1(a)], the spin quantum number S critically determines the magnitude of quantum spin fluctuations of a long-wavelength mode $\boldsymbol{n}(\tau, x)$ around a short-range Néel order. The topological Berry-phase term gives a contribution of $S^{\mathrm{B}}_{\mathrm{1DHAF}} = i2\pi SQ$ to a nonlinear-σ model action for $\boldsymbol{n}$ with a topological integer $Q = \frac{1}{4\pi}\int_0^{1/T} d\tau \int dx\, \boldsymbol{n}\cdot(\frac{\partial \boldsymbol{n}}{\partial x}\times\frac{\partial \boldsymbol{n}}{\partial \tau})$ and the temperature T. Thus, $e^{-S^{\mathrm{B}}_{\mathrm{1DHAF}}}$ can take -1 for a half-integer S, allowing for gapless excitations from a disordered ground state. On the other hand, it is always unity for an integer S, leading to a so-called Haldane gap [2,3] in the $S = 1$ excitation spectrum from a nonmagnetic ground state [4,5], as experimentally evidenced in $Ni(C_2H_8N_2)_2NO_2(ClO_4)$ (NENP)[6–8].

In the presence of an antiferromagnetic second-neighbor exchange coupling J_2, however, the above simple arguments no longer hold. In particular, quasi-1D spin-$\frac{1}{2}$ multiferroic and/or magnetoelectric edge-sharing cuprates, such as $LiCu_2O_2$ [9,10], $LiCuVO_4$ [11,12], $PbCuSO_4(OH)_2$ [13,14], and $Rb_2Cu_2Mo_3O_{12}$ [15–17], involve a ferromagnetic J_1 because of nearly 90° Cu-O-Cu bond angles, in addition to an antiferromagnetic second-neighbor exchange coupling J_2. The J_1-J_2 frustrated spin-$\frac{1}{2}$ Heisenberg chain accommodates a dimerized spin-singlet short-range resonating valence bond ground state [18,19]. This state is formed by emergent spin-1 pairs [Fig. 1(b)] and has an extremely small Haldane gap and incommensurate short-range spin correlations. Weak but finite easy-plane exchange magnetic anisotropy then induces a quasi-long-range gapless incommensurate spin-spiral and long-range vector spin chirality ($\sum_\ell \langle \boldsymbol{S}_\ell \times \boldsymbol{S}_{\ell+1}\rangle$) [20] orders [19,21]. A coexisting phase of the vector spin chirality order and the Haldane gap also appears in between the two phases [22]. These states are, however, readily driven to a long-range spiral magnetic order by three-dimensional couplings. This scenario elucidates the ferroelectricity due to the cycloidal magnetism in $LiCu_2O_2$ [10], $LiCuVO_4$ [12], and $PbCuSO_4(OH)_2$ [13].

In fact, the ferroelectricity associated with the vector spin chirality order may appear robustly in the vector-chiral Haldane dimer phase without the long-range spiral magnetism, if the spin gap is enhanced [23] so that it dominates over the interchain interactions. Indeed, $Rb_2Cu_2Mo_3O_{12}$ provides a unique example of a field-induced ferroelectricity hosted by a nonmagnetic ground state with a spin gap [16,17]. A recent muon spin relaxation (μSR) study also indicates the formation of a spin-singlet state on cooling below $\sim$7 K and saturation at around 1–2 K [24]. In this Rapid Communication,

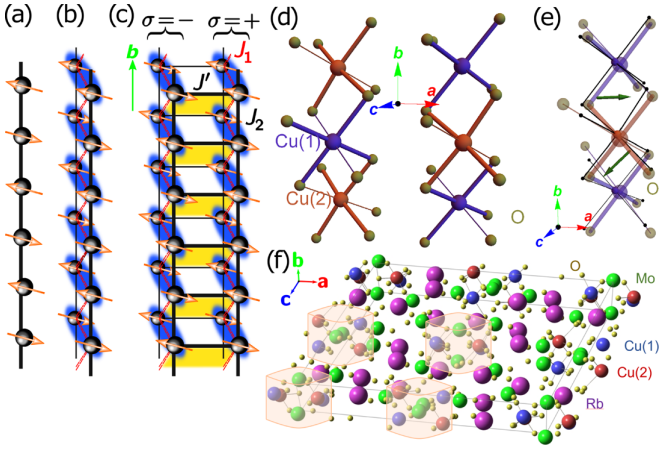

FIG. 1. Structures of spin chains. (a) Antiferromagnetic spin chain. (b) Frustrated spin-$\frac{1}{2}$ chain with emergent spin-1 pairs (blue clouds). Solid (broken) lines represent antiferromagnetic (ferromagnetic) interactions. (c) Short-range resonating valence bond state involving tetramers (yellow plaquettes) connecting emergent spin-1 pairs. (d) Crystal structure of a pair of spin-$\frac{1}{2}$ chains comprising edge-sharing distorted CuO_6 octahedra in $Rb_2Cu_2Mo_3O_{12}$. (e) An ideal centrosymmetric chain of edge-sharing regular CuO_6 octahedra (black points), compared with the noncentrosymmetric one in $Rb_2Cu_2Mo_3O_{12}$. Electric dipole moments due to ionic displacements are shown on the first-neighbor Cu spin pairs by dark green arrows. (f) A unit cell of $Rb_2Cu_2Mo_3O_{12}$. Two-leg ladders are located in translucent orange tubes.

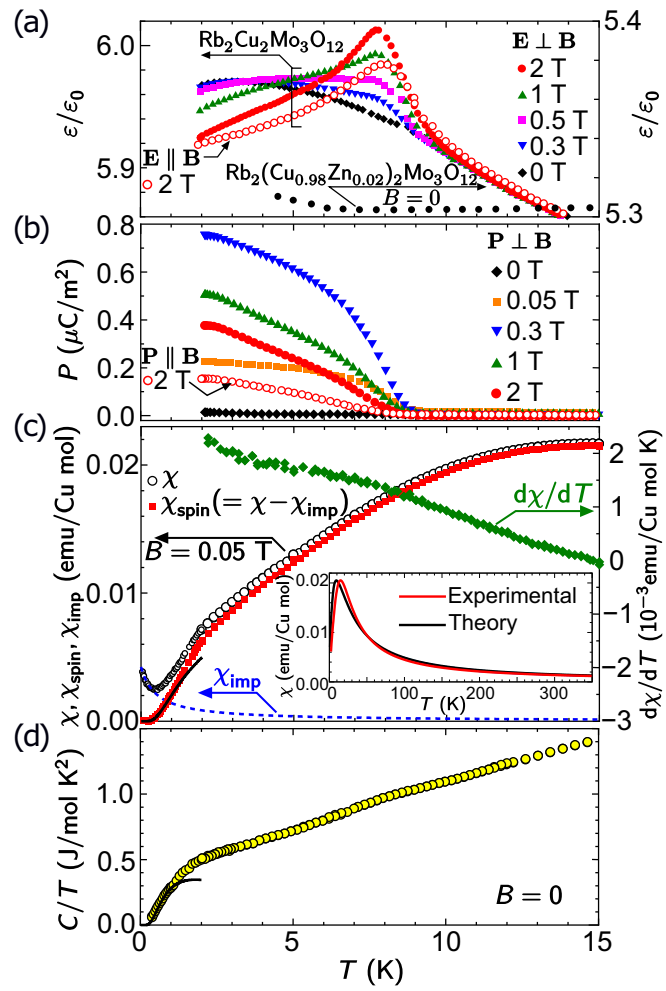

FIG. 2. Temperature dependence of thermodynamic properties of polycrystalline $Rb_2Cu_2Mo_3O_{12}$. (a) Dielectric constant $\varepsilon/\varepsilon_0$. (b) Electric polarization P at magnetic fields. Note that a powder average of the magnetic field direction broadens the transition. (c) Magnetic susceptibility χ (open circles). The impurity contribution χ_{imp}, responsible for the upturn of χ below 0.5 K, was fitted by the Curie-Weiss law with the spin vacancy concentration of 0.5% and the Weiss temperature -0.5 K (blue dashed curve). Red points represent the data χ_{spin} subtracted by χ_{imp}. Also shown is $d\chi/dT$ (green points). The inset shows a high-temperature fitting of χ (black curve) with a powder average of the exact diagonalization results (red curve). (d) Specific heat C at $B = 0$. The solid curves in (c) and (d) are the fitting curves proportional to $\exp(-E_g/T)$ with the energy gap $E_g = 1.7$ K.

we report combined experimental and theoretical evidence that in the quasi-1D cuprate $Rb_2Cu_2Mo_3O_{12}$, a Haldane-gap ground state formed by emergent spin-1 pairs of $S = \frac{1}{2}$ Cu spins [Fig. 1(c)] harbors a ferroelectricity stabilized by a tiny magnetic field.

Figures 2 shows a temperature dependence of thermodynamic properties of polycrystalline $Rb_2Cu_2Mo_3O_{12}$ samples. The dielectric constant ε gradually increases on cooling. Then, as in most magnetically induced ferroelectrics, it exhibits a kink for $B = 0.3$ and 0.5 T or a peak for $B = 1$ and 2 T at around 8 K [Fig. 2(a)], below which the electric polarization P emerges at an even weaker magnetic field $B = 0.05$ T [Fig. 2(b)]. Thus, the anomaly in ε at $B \geqslant 0.05$ T should be ascribed to a ferroelectric transition at $T_{FE} \sim 8$ K. It is natural to expect that the ferroelectric polarization persists at $T < 2$ K because of no sign of a reentrant behavior in ε and P in the low-temperature range. Remarkably, ε does not show a significant decay on cooling down to 2 K for $B \leqslant 0.5$ T, while it does for $B \geqslant 1$ T. Furthermore, doping nonmagnetic Zn impurities into Cu sites by 2% [25] drastically suppresses ε and removes the anomaly associated with the ferroelectric transition [Fig. 2(a)]. Therefore, it is clear that the ferroelectricity is indeed triggered by a coherence in the spin degrees of freedom under the weak magnetic field.

The signals of both ε and P below T_{FE} are larger for the configuration of $\boldsymbol{E}, \boldsymbol{P} \perp \boldsymbol{B}$ than for $\boldsymbol{E}, \boldsymbol{P} \parallel \boldsymbol{B}$ at least at 2 T [Figs. 2(a) and 2(b)], as in many edge-sharing multiferroic cuprates showing a cycloidal magnetic order [10,12,13]. This implies that the uniform vector spin chirality gives rise to a dominant contribution to the ferroelectric polarization among many mechanisms [26]. On the other hand, no anomaly is observed in the magnetic susceptibility χ and $d\chi/dT$ [Fig. 2(c)], in contrast to the multiferroic cuprates [10,12,13]. Moreover, a spin gap $E_g \sim 1.7$ K has been observed in both χ and the specific heat C [16,17] [Figs. 2(c) and 2(d)].

The emergence of this spin gap is also confirmed by the measurements of the magnetization M. Figures 3(a) and 3(b) present experimental results on M and on dM/dB and d^2M/dB^2, respectively. A subtraction of a small impurity contribution as outlined in Fig. 2 caption reveals that M at $T = 0.08$ K shows an activation by the threshold field $B_c \sim 2.0$ T where d^2M/dB^2 exhibits a peak. On the other hand, at a much

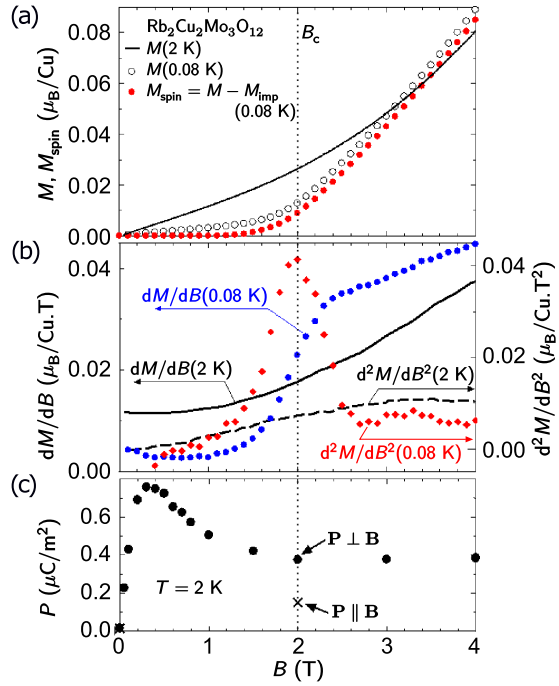

FIG. 3. Magnetic field dependence of thermodynamic properties of polycrystalline $Rb_2Cu_2Mo_3O_{12}$. (a) Magnetization M per Cu atom. (b) Derivatives of M with respect to B. (c) Ferroelectric polarization P for both $\boldsymbol{P} \parallel \boldsymbol{B}$ and $\boldsymbol{P} \perp \boldsymbol{B}$.

lower temperature $T = 2.0$ K than T_{FE}, $\boldsymbol{P}(\perp \boldsymbol{B})$ steeply appears at a much lower field, at least 0.03 T, than B_c [Fig. 3(c)]. It exhibits a broad peak at around 0.2–0.3 T, and then gradually decays to a constant at higher fields up to 4 T. This observation confirms that the ferroelectricity is stabilized by a tiny magnetic field but not affected by a closing of the spin gap and an onset of the magnetization at B_c. Namely, at the energy scale associated with 0.03 T or less, there exists a low-energy mode, which is magnetic-dipole inactive but electric-dipole active, and thus linearly coupled to the vector spin chirality.

All the above thermodynamic properties provide evidence of a spin-gapped ferroelectric behavior stabilized by the tiny applied magnetic field, most likely through the vector spin chirality. It should also be possible to confirm this from spectral properties. To probe $S = 1$ triplet excitations from the nonmagnetic ground state, low-energy inelastic neutron-scattering experiments have been performed on powder samples. Figure 4(a) represents the results at 1.5 K measured on the AMATERAS spectrometer. Discrete excited levels are clearly seen at 0.2, 0.38, and 0.6 meV. The periodicity of these spin excitations along the chain can be determined from the onset wavenumber $Q \sim 0.3$ Å^{-1} of the powder-averaged intensities, and roughly corresponds to eight spins. A natural interpretation will be that $S = 1$ triplet excitations are split into the three by Dzyaloshinskii-Moriya interactions. Note that cooling below T_{FE} and applying the magnetic field do not alter the diffraction patterns (Fig. 4(f) and Ref. [28]): neither a superlattice peak nor any visible additional diffraction intensity appears. Note also that a clear long-range magnetic order is absent at the incommensurate wavevector $(0, Q_b, 0)$ to an accuracy of $0.06\mu_B$. Actually,

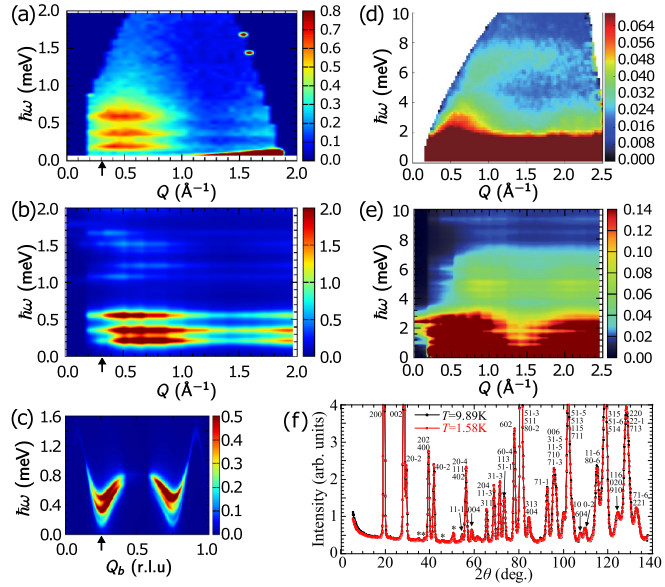

FIG. 4. Neutron-scattering results on polycrystalline $Rb_2Cu_2Mo_3O_{12}$ at $B = 0$. (a) Experimental and (b) theoretical low-energy powder-averaged spectra, measured at 1.6 K and calculated at $T = 0$, respectively. (c) Theoretical low-energy spectra along the b axis without the powder average. The results obtained from a 28-site cluster by taking the parameter set for the thermodynamic limit [27] have been interpolated. The incommensurate wavevector $Q = 0.3$ Å^{-1} is marked by black arrows in (a), (b), and (c). (d) Experimental and (e) theoretical powder-averaged spectra, measured at 6.5 K and calculated at $T = 0$, respectively, in a wider energy range. Note that the incommensurate wavevector is shifted downwards from the maximum position of the powder-averaged spectra to the onset in the panels (a) and (b). (f) Neutron powder diffraction patterns of $Rb_2Cu_2Mo_3O_{12}$ measured at 9.89 K $> T_{FE}$ (black) and 1.58 K $< T_{FE}$ (red) in $B = 0$ T. The four peaks with $*$ symbols are derived from a nonmagnetic impurity phase $Rb_2Mo_3O_{10}$. A cold neutron wavelength $\lambda = 4.5$ Å was chosen.

the absence of clear muon spin precession or relaxation [24] precludes a long-range order of all the Cu spins with moment amplitude $\gtrsim 0.01\mu_B$ and of dilute (>1%) Cu or impurity spins with moment amplitude $1\mu_B$. The possibility of having a tiny fraction (<1%) of magnetically ordered domains in the polycrystalline samples can hardly be ruled out. However, such order is absolutely extrinsic and irrelevant to the observed magnetic and ferroelectric properties of the bulk, because the Weiss temperature -0.5 K is much lower than T_{FE} and the exchange coupling constants obtained below.

The overall experimental results on the magnetic properties can be elucidated theoretically from the following two-leg ladder model of frustrated J_1-J_2 spin-$\frac{1}{2}$ chains [Fig. 1(c)] [27]:

$$H = \sum_{\ell}\sum_{\sigma=\pm}\Bigg[\sum_{j=1,2} J_j \boldsymbol{S}_{\sigma,\ell}\cdot\boldsymbol{S}_{\sigma,\ell+j} + J'\boldsymbol{S}_{+,\ell}\cdot\boldsymbol{S}_{-,\ell}, + \sigma((-1)^{\ell}\boldsymbol{D}_{\mathrm{s}}\cdot\boldsymbol{S}_{\sigma,\ell}\times\boldsymbol{S}_{\sigma,\ell+1} + \boldsymbol{D}_{\mathrm{u}}\cdot\boldsymbol{S}_{\sigma,\ell}\times\boldsymbol{S}_{\sigma,\ell+1}) - g\mu_B\boldsymbol{B}\cdot\boldsymbol{S}_{\sigma,\ell}\Bigg] \quad (1)$$

with the g factor $g = 2.16$ [27] and the applied magnetic field $\boldsymbol{B}$, where $\boldsymbol{S}_{\sigma,\ell}$ stands for an $S = \frac{1}{2}$ spin at the site ℓ in the chain of edge-shared CuO_6 octahedra [Fig. 1(d)] labeled by the index $\sigma = \pm$. It has already been revealed that the antiferromagnetic rung exchange coupling J' between the nearest-neighbor spins in the adjacent J_1-J_2 chains is required for enhancing the spin gap [29]. $\boldsymbol{D}_{\rm u}$ and $\boldsymbol{D}_{\rm s}$ represent the uniform and staggered components of intrachain Dzyaloshinskii-Moriya vectors caused by two inequivalent first-neighbor Cu-Cu bonds involving noncollinear electric dipole moments, as shown by dark green arrows in Fig. 1(e). No crystal symmetry constrains the directions of the Dzyaloshinskii-Moriya vectors. However, since the numerical results shown below are insensitive to a nonzero value of $\boldsymbol{D}_{\rm u} \cdot \boldsymbol{D}_{\rm s}$, we take $\boldsymbol{D}_{\rm u} \perp \boldsymbol{D}_{\rm s}$. Henceforth, we adopt $J_1 = -114\,{\rm K}$, $J_2 = 35.1\,{\rm K}$, $J' = 20.5\,{\rm K}$, $D_{\rm s} = 44.3\,{\rm K}$, and $D_{\rm u} = 24.4\,{\rm K}$ to explain overall results of the magnetic susceptibility and inelastic neutron-scattering spectra from exact-diagonalization calculations on a 16-site cluster. [See Supplemental Material [27] for examinations of finite-size effects by means of the density-matrix renormalization group for infinite systems (iDMRG).] Indeed, the numerical results on χ for $B = 0$ reasonably agree with the experimental data [15], as shown in the inset of Fig. 2(c), and the iDMRG result 2.15 T on the critical magnetic field agrees with the experimental one $\sim$2.0 T [Fig. 3(b)]. Furthermore, the experimental results on the low-energy powder-averaged inelastic neutron-scattering spectra [Fig. 4(a)] are nicely explained by the theoretical results [Fig. 4(b)] [27]. From Figs. 4(a) and 4(b), the three low-energy excitations might look dispersionless. However, this is an artifact of powder averaging. Figure 4(c) shows the theoretical results of the dispersive spectra as a function of the particular wavevector component Q_b in the chain direction, the crystallographic b axis, with $Q_a = Q_c = 0$. Actually, the agreement in the inelastic neutron-scattering spectra extends to a much higher energy $\sim$10 meV, as is apparent by comparing the current experimental results in the high energy range measured at the 4SEASONS spectrometer [Fig. 4(d)], which are refined from the previous data [30], with the theoretical results [27] [Fig. 4(e)].

The scenario of a splitting of the $S = 1$ excited states due to Dzyaloshinskii-Moriya interactions is also supported by electron spin resonance (ESR) experiments on powder samples. Figure 5(a) presents the temperature dependence of the ESR transmission spectra at a frequency $f = 81$ GHz $\sim$ 0.33 meV as a function of B. A paramagnetic resonance is found as a significantly broad peak at 2.7 T for a much lower temperature, 8.7 K, than J_1, J_2, and J', as indicated by red arrows. It should appear as a much sharper peak in the absence of moderately large Dzyaloshinskii-Moriya interactions [31]. On cooling, the peak becomes even more broadened, and eventually bifurcates below 5 K. In the frequency dependence of the ESR spectra at 1.6 K [Fig. 5(b)], this new low-energy mode (green arrows) has been identified, as well as another lower-energy mode (blue arrows). These two modes are plotted with $\triangle$ and $\triangledown$ in the B-f diagram of Fig. 5(c), in favorable comparison with a density plot of the theoretical results [27] on the optical absorption power [32] at the same temperature. The dominant contributions to the two series originate from thermally activated transitions.

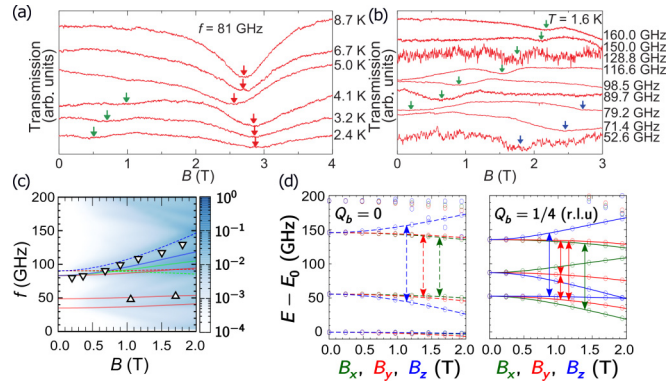

FIG. 5. Electron spin resonance spectra of polycrystalline $Rb_2Cu_2Mo_3O_{12}$. (a) Temperature dependence of the experimental transmission spectra at 81 GHz. Arrows represent the resonance fields. (b) Experimental transmission spectra at 1.6 K for designated frequencies. Green and blue arrows denote two sequences of resonance fields. (c) Theoretical optical absorption power at 1.6 K. Experimentally observed resonance fields indicated by blue and green arrows in (a) are plotted by $\triangle$ and $\triangledown$, respectively, for comparison. (d) Energy levels at $Q_b = 0$ (left) and $Q_b = 1/4$ r.l.u. (right) computed under $\boldsymbol{B}$ applied along the x, y, and z directions, where $\boldsymbol{D}_u \parallel z$ and $\boldsymbol{D}_s \parallel x$. Transitions denoted by the arrows in the left (right) panel produce resonance spectra shown by dashed (solid) curves in (c).

Theoretically, the second-lowest-energy mode ($\triangledown$) is ascribed to transitions from the first excited state to the third at the wavevector $Q_b = 1/4$ r.l.u. [the right panel of Fig. 5(d)] and from the first excited state to the second at $Q_b = 0$ [the left panel of Fig. 5(d)], as shown by solid and dashed curves in Fig. 5(c), respectively. The lowest-energy mode ($\triangle$) is ascribed to transitions from the first excited state to the second and from the second to the third at $Q_b = 1/4$ r.l.u. [the right panel of Fig. 5(d)], as shown by two solid curves in Fig. 5(c). A significantly large dependence of the excitation energies on the field direction in the theoretical calculations shown in Fig. 5(d) also elucidates the unusually broad spectral features identified in the powder ESR experiments.

The current frustrated spin-$\frac{1}{2}$ ladder model, that has reproduced overall experimental results on $Rb_2Cu_2Mo_3O_{12}$, actually has a tetramer-singlet ground state formed by emergent $S = 1$ spins with a Haldane gap. [See Fig. 1(c).] This ground state is adiabatically connected to the limit of the two decoupled chains with $J' = 0$, each of which has a singlet Haldane dimer ground state [22], and then to the two decoupled spin-1 Haldane chains, as in an antiferromagnetic spin-1 ladder [33]. At present, it remains open to explain the ferroelectricity stabilized by a tiny magnetic field. Nevertheless, it is clear from the symmetry that it is accompanied by a genuine long-range vector spin chirality order, which is not parasitic to a (quasi-)long-range spiral magnetic order. This ground state has long been sought since the proposal by Villain [20]. Thus, the current study uncovers a unique class of magnetically induced ferroelectricity in the absence of a long-range magnetic order, in contrast to many multiferroic magnets due to a cycloidal magnetism. A quest for additional microscopic properties of this ferroelectric (vector-spin-chirality ordered) emergent

Haldane-gap state will require experiments on single crystals and the associated microscopic theoretical analyses.

The authors acknowledge I. Terasaki for his support of the work and helpful discussion and K. Kaneko for preliminary neutron scattering experiments on the triple-axis spectrometer LTAS installed at the JRR-3 reactor, Japan. Numerical calculations were partially performed by using the RIKEN Integrated Cluster of Clusters and the RIKEN HOKUSAI supercomputers. The time-of-flight neutron-scattering experiments were performed using the chopper spectrometers AMATERAS and 4SEASONS at J-PARC (Proposals No. 2012P0202 and No. 2009A0093). The work was partially supported by Grants-in-Aid for Scientific Research (Grants 24244059, 24740253, 25220803, 25246006, 25800221, 16K05426, 17001001, 17H06137, and 17K14359) from the Japan Society for the promotion of Science, by the RIKEN iTHES project, by the FRIS Program for the creation of interdisciplinary research at Tohoku University, and by Swiss National Science Foundation via the SNSF project, Grant No. 200021_153451. The neutron-diffraction experiments were performed at the Swiss spallation neutron source SINQ, Paul Scherrer Institute, Villigen, Switzerland. H.U. is grateful to S. Yunoki for his support.

[1] P. W. Anderson, Mater. Res. Bull. **8**, 153 (1973).
[2] F. Haldane, Phys. Lett. A **93**, 464 (1983).
[3] F. D. M. Haldane, Phys. Rev. Lett. **50**, 1153 (1983).
[4] E. Lieb, T. Schultz, and D. Mattis, Ann. Phys. (NY) **16**, 407 (1961).
[5] I. Affleck, J. Phys.: Condens. Matter **1**, 3047 (1989).
[6] J. P. Renard, M. Verdaguer, L. P. Regnault, W. A. C. Erkelens, J. Rossat-Mignod, and W. G. Stirling, Europhys. Lett. **3**, 945 (1987).
[7] K. Katsumata, H. Hori, T. Takeuchi, M. Date, A. Yamagishi, and J. P. Renard, Phys. Rev. Lett. **63**, 86 (1989).
[8] M. Hagiwara, K. Katsumata, I. Affleck, B. I. Halperin, and J. P. Renard, Phys. Rev. Lett. **65**, 3181 (1990).
[9] T. Masuda, A. Zheludev, B. Roessli, A. Bush, M. Markina, and A. Vasiliev, Phys. Rev. B **72**, 014405 (2005).
[10] S. Park, Y. J. Choi, C. L. Zhang, and S.-W. Cheong, Phys. Rev. Lett. **98**, 057601 (2007).
[11] M. Enderle, C. Mukherjee, B. Fåk, R. K. Kremer, J.-M. Broto, H. Rosner, S.-L. Drechsler, J. Richter, J. Malek, A. Prokofiev, W. Assmus, S. Pujol, J.-L. Raggazzoni, H. Rakoto, M. Rheinstädter, and H. M. Rønnow, Europhys. Lett. **70**, 237 (2005).
[12] Y. Naito, K. Sato, Y. Yasui, Y. Kobayashi, Y. Kobayashi, and M. Sato, J. Phys. Soc. Jpn. **76**, 023708 (2007).
[13] Y. Yasui, M. Sato, and I. Terasaki, J. Phys. Soc. Jpn. **80**, 033707 (2011).
[14] A. U. B. Wolter, F. Lipps, M. Schäpers, S.-L. Drechsler, S. Nishimoto, R. Vogel, V. Kataev, B. Büchner, H. Rosner, M. Schmitt, M. Uhlarz, Y. Skourski, J. Wosnitza, S. Süllow, and K. C. Rule, Phys. Rev. B **85**, 014407 (2012).
[15] M. Hase, H. Kuroe, K. Ozawa, O. Suzuki, H. Kitazawa, G. Kido, and T. Sekine, Phys. Rev. B **70**, 104426 (2004).
[16] Y. Yasui, Y. Yanagisawa, R. Okazaki, I. Terasaki, Y. Yamaguchi, and T. Kimura, J. Appl. Phys. **113**, 17D910 (2013).
[17] Y. Yasui, R. Okazaki, I. Terasaki, M. Hase, M. Hagihala, T. Masuda, and T. Sakakibara, JPS Conf. Proc. **3**, 014014 (2014).
[18] C. Itoi and S. Qin, Phys. Rev. B **63**, 224423 (2001).
[19] S. Furukawa, M. Sato, and S. Onoda, Phys. Rev. Lett. **105**, 257205 (2010).
[20] J. Villain, Ann. Isr. Phys. Soc. **2**, 565 (1978).
[21] A. A. Nersesyan, A. O. Gogolin, and F. H. L. Eßler, Phys. Rev. Lett. **81**, 910 (1998).
[22] S. Furukawa, M. Sato, S. Onoda, and A. Furusaki, Phys. Rev. B **86**, 094417 (2012).
[23] H. Ueda and S. Onoda, Phys. Rev. B **90**, 214425 (2014).
[24] S. Ohira-Kawamura, K. Tomiyasu, A. Koda, D. P. Sari, R. Asih, S. Yoon, I. Watanabe, and K. Nakajima, JPS Conf. Proc. **21**, 011007 (2018).
[25] Y. Yasui, Y. Yanagisawa, R. Okazaki, and I. Terasaki, Phys. Rev. B **87**, 054411 (2013).
[26] C. Jia, S. Onoda, N. Nagaosa, and J. H. Han, Phys. Rev. B **76**, 144424 (2007).
[27] See Supplemental Material at http://link.aps.org/supplemental/10.1103/PhysRevB.101.140408 for examinations of finite-size effects by means of the density-matrix renormalization group for infinite systems (iDMRG). See also Refs. [34–49].
[28] N. Reynolds, A. Mannig, H. Luetkens, C. Baines, T. Goko, R. Scheuermann, L. Keller, M. Bartkowiak, A. Fujimura, Y. Yasui, C. Niedermayer, and J. S. White, Phys. Rev. B **99**, 214443 (2019).
[29] H. Ueda and S. Onoda, arXiv:2003.00554.
[30] K. Tomiyasu, M. Fujita, A. I. Kolesnikov, R. I. Bewley, M. J. Bull, and S. M. Bennington, Appl. Phys. Lett. **94**, 092502 (2009).
[31] A. Zorko, D. Arčon, H. van Tol, L. C. Brunel, and H. Kageyama, Phys. Rev. B **69**, 174420 (2004).
[32] C. Slichter, *Principles of Magnetic Resonance*, Springer Series in Solid-State Sciences (Springer-Verlag, Berlin, 1990).
[33] S. Todo, M. Matsumoto, C. Yasuda, and H. Takayama, Phys. Rev. B **64**, 224412 (2001).
[34] S. F. Solodovnikov and Z. A. Solodovnikova, J. Struct. Chem. **38**, 765 (1997).
[35] H. Ueda and S. Onoda, Phys. Rev. B **89**, 024407 (2014).
[36] C. E. Agrapidis, S.-L. Drechsler, J. van den Brink, and S. Nishimoto, Phys. Rev. B **95**, 220404(R) (2017).
[37] C. Efthimia Agrapidis, S.-L. Drechsler, J. van den Brink, and S. Nishimoto, SciPost Phys. **6**, 019 (2019).
[38] S. R. White, Phys. Rev. Lett. **69**, 2863 (1992).
[39] S. R. White, Phys. Rev. B **48**, 10345 (1993).
[40] I. P. McCulloch, arXiv:0804.2509.
[41] J. Cullum and W. E. Donath, in *Proceedings of the 1974 IEEE Conference on Decision and Control, November 20–22, Phoenix* (IEEE, New York, 1974), pp. 505–509.
[42] R. Haydock, V. Heine, and M. J. Kelly, J. Phys. C **5**, 2845 (1972).
[43] E. R. Gagliano and C. A. Balseiro, Phys. Rev. Lett. **59**, 2999 (1987).
[44] E. Dagotto, Rev. Mod. Phys. **66**, 763 (1994).

[45] W. H. Press, S. A. Teukolsky, W. T. Vetterling, and B. P. Flannery, *Numerical Recipes in Fortran 90: The Art of Parallel Scientific Computing*, 2nd ed. (Cambridge University Press, New York, 1996).

[46] K. Nakajima, S. Ohira-Kawamura, T. Kikuchi, M. Nakamura, R. Kajimoto, Y. Inamura, N. Takahashi, K. Aizawa, K. Suzuya, K. Shibata, T. Nakatani, K. Soyama, R. Maruyama, H. Tanaka, W. Kambara, T. Iwahashi, Y. Itoh, T. Osakabe, S. Wakimoto, K. Kakurai, F. Maekawa, M. Harada, K. Oikawa, R. E. Lechner, F. Mezei, and M. Arai, J. Phys. Soc. Jpn. **80**, SB028 (2011).

[47] R. Kajimoto, M. Nakamura, Y. Inamura, F. Mizuno, K. Nakajima, S. Ohira-Kawamura, T. Yokoo, T. Nakatani, R. Maruyama, K. Soyama, K. Shibata, K. Suzuya, S. Sato, K. Aizawa, M. Arai, S. Wakimoto, M. Ishikado, S. Shamoto, M. Fujita, H. Hiraka, K. Ohoyama, K. Yamada, and C.-H. Lee, J. Phys. Soc. Jpn. **80**, SB025 (2011).

[48] Y. Inamura, T. Nakatani, J. Suzuki, and T. Otomo, J. Phys. Soc. Jpn. **82**, SA031 (2013).

[49] J. Schefer, P. Fischer, H. Heer, A. Isacson, M. Koch, and R. Thut, Nucl. Instrum. Methods Phys. Res. Sect. A **288**, 477 (1990).